Osteoarthritis and Cartilage 27 (2019) 1309–1314

Osteoarthritis and Cartilage

Brief Report

# Dual-energy computed tomography in calcium pyrophosphate deposition: initial clinical experience

T. Pascart † ‡ *, L. Norberciak §, J. Legrand ‖, F. Becce ¶ [a], J.-F. Budzik ‡ ‖ [a]

† Department of Rheumatology, Lille Catholic Hospitals, University of Lille, F-59160 Lomme, France
‡ EA 4490, PMOI, Physiopathologie des Maladies Osseuses Inflammatoires, University of Lille, Lille, France
§ Department of Medical Research, Biostatistics, Lille Catholic Hospitals, University of Lille, Lomme, France
‖ Department of Diagnostic and Interventional Radiology, Lille Catholic Hospitals, University of Lille, Lomme, France
¶ Department of Diagnostic and Interventional Radiology, Lausanne University Hospital and University of Lausanne, Lausanne, Switzerland

ARTICLE INFO

*Article history:*
Received 1 October 2018
Accepted 1 May 2019

*Keywords:*
Dual-energy computed tomography
Calcium pyrophosphate deposition
Calcium hydroxyapatite
Chondrocalcinosis
Knee
Meniscus

SUMMARY

*Objective:* To determine the dual-energy computed tomography (DECT) attenuation properties of meniscal calcifications in calcium pyrophosphate deposition (CPPD) *in vivo*, and assess whether DECT was able to discriminate meniscal CPP deposits from calcium hydroxyapatite (HA) in subchondral and trabecular bone.

*Method:* Patients with clinical suspicion of crystal-related arthropathy (gout and/or CPPD) and knee DECT scans were retrospectively assigned to CPPD ($n = 19$) or control ($n = 21$) groups depending on the presence/absence of chondrocalcinosis on DECT. Two observers drew standardized regions of interest (ROI) in meniscal calcifications, non-calcified menisci, as well as subchondral and trabecular bone. Five DECT parameters were obtained: CT numbers (HU) at 80 and 140 kV, dual-energy index (DEI), electron density ($\rho_e$), and effective atomic number ($Z_{eff}$). The four different knee structures were compared within/between patients and controls using linear mixed models, adjusting for confounders.

*Results:* Meniscal calcifications ($n = 89$) in CPPD patients had mean ± SD CT numbers at 80 and 140 kV of 257 ± 64 and 201 ± 48 HU, respectively; with a DEI of 0.023 ± 0.007, and $\rho_e$ and $Z_{eff}$ of 140 ± 35 and 8.8 ± 0.3, respectively. Meniscal CPP deposits were readily distinguished from calcium HA in subchondral and trabecular bone ($p \leq 0.001$), except at 80 kV separately ($p = 0.74$). $Z_{eff}$ and $\rho_e$ both significantly differed between CPP deposits and calcium HA in subchondral and trabecular bone ($p < 0.0001$).

*Conclusion:* This proof-of-concept study shows that DECT has the potential to discriminate meniscal CPP deposits from calcium HA in subchondral and trabecular bone *in vivo*, paving the way for the non-invasive biochemical signature assessment of intra- and juxta-articular calcium crystal deposits.



## Introduction

Calcium pyrophosphate (CPP) deposition (CPPD) can be associated with acute and chronic arthritis[1], as well as osteoarthritis (OA) progression[1,2]. The reference standard for the diagnosis of CPP arthritis remains crystal identification in synovial fluid aspirates using compensated polarized light microscopy[3]. The sensitivity of CPP crystal identification is however lower than in gout, and calcium pyrophosphate deposition (CPPD) diagnosis without crystal confirmation remains challenging[3,4]. Radiographic chondrocalcinosis and clinical assessment may be sufficient to retain a probable diagnosis of CPP crystal arthritis[3]. However, calcium compounds attenuate a polychromatic X-ray beam in a similar fashion, regardless of whether they are part of a soft-tissue CPP or calcium hydroxyapatite (HA) deposit, or calcium phosphate bone lattice. Moreover, the classic radiographic appearance of the various calcifications (linear for CPP vs amorphous and cloud-like for calcium HA) does not always allow accurate distinction[5], even when applying the compartment-based musculoskeletal approach[6]; CPP deposits being more frequently found intra-articularly (fibrocartilage and hyaline cartilage), while calcium HA predominates around joints and in bones[5].

* Address correspondence and reprint requests to: T. Pascart, Saint-Philibert Hospital, Rue du Grand But, 59160, Lomme, France. Tel.: 33-3 20-22-50-59; Fax: 33-20-22-38-76.
*E-mail addresses:* pascart.tristan@ghicl.net (T. Pascart), norberciak.laurene@ghicl.net (L. Norberciak), legrand.julie@ghicl.net (J. Legrand), fabio.becce@chuv.ch (F. Becce), budzik.jean-francois@ghicl.net (J.-F. Budzik).
[a] F. Becce and J.-F. Budzik contributed equally to this work.

https://doi.org/10.1016/j.joca.2019.05.007
1063-4584/

Dual-energy computed tomography (DECT) is based on the principle that tissue attenuation, which is reflected by CT numbers (in Hounsfield unit, HU), depends on volumetric mass density, material composition (reflected by the effective atomic number, $Z_{eff}$), and X-ray beam energy (in keV)[7]. This technique offers the possibility to determine the molecular signature of biochemical compounds. Over the past decade, DECT has been used increasingly to discriminate monosodium urate (MSU) from calcium deposits in gout[8]. This led to progress in the diagnosis and severity assessment of gout, and DECT is being evaluated as a potential tool for disease monitoring[9]. Although similar advances can be expected for CPPD, the potential of DECT for detecting and most importantly characterizing calcium crystal deposition has not yet been explored *in vivo*[10].

Therefore, our objectives were, first, to determine the DECT attenuation properties of meniscal calcifications in CPPD *in vivo*, and second, to assess whether DECT was able to discriminate meniscal CPP deposits from calcium HA in subchondral and trabecular bone.

## Method

### *Patients and study design*

Patients with clinical suspicion of acute and/or chronic crystal-related arthropathy (gout and/or CPPD according to 2015 ACR/EULAR gout classification criteria[11] and 2011 EULAR CPPD recommendations[3], respectively) were prospectively screened from April 2016 to March 2018, and 78 subjects finally enrolled to undergo DECT scans of their knees. Additional details on the study originally designed for gout are reported elsewhere[12]. From these 78 patients, we retrospectively retrieved all those with chondrocalcinosis on knee DECT scans and assigned them to the CPPD group ($n = 19$). A control group of 21 patients without knee DECT chondrocalcinosis and prior acute CPP crystal arthritis was then randomly selected among remaining subjects. This study was approved by the institutional review board of Lille Catholic University Hospitals (protocol 2016-04-16), and all patients provided written informed consent.

### *DECT protocol*

DECT scans were performed using a novel single-source CT system (Somatom Definition Edge; Siemens Healthineers, Erlangen, Germany). TwinBeam Dual Energy is the latest DECT technology that enables to create two X-ray spectra simultaneously from a single tube. The X-ray beam is pre-filtered using two different materials: gold (Au) and tin (Sn). As a result, the 120 kV beam is split into high- (Sn) and low-energy (Au) X-ray spectra before being attenuated by the patient[13]. Knees were scanned jointly in the axial plane, with patients positioned supine. Data were acquired using the following parameters: tube potentials, 80 and 140 kV; quality reference tube current-time products at 80 and 140 kV, 125–216 and 30–55 mAs, respectively; beam collimation, 128 × 0.6 mm; pitch, 0.7; overall volume CT dose indexes, 5.6–12.3 mGy. Images were then reconstructed as follows: section thickness/overlap, 0.75/0.25 mm; field of view, 300 × 300 (±20) mm, yielding in-plane pixel sizes of 0.55 × 0.55–0.63 × 0.63 mm; both smooth (B30f) and sharp (B70f) kernels.

### *Image analysis*

DECT images were post-processed and analyzed on a dedicated workstation using the DE Rho/Z software (syngo.via VB10B; Siemens Healthineers). A rheumatologist experienced in crystal-related arthropathies drew freehand regions of interest (ROI) on preset (except for meniscal calcifications) coronal-oblique-reformatted grayscale DECT images of all right tibiofemoral joints, which were then copied-pasted on DE Rho/Z maps. Separate standardized ROIs were positioned in meniscal calcifications (the largest of each meniscal segment, when present), non-calcified menisci (one each in anterior, middle and posterior segments of medial and lateral menisci), as well as subchondral and trabecular bone (Supplementary Fig. 1). Meniscal calcifications were fully encompassed and their cross-sectional area noted, while taking care to avoid partial volume effects. The size of other ROIs ranged between 0.3 and 0.5 $cm^2$ depending on the anatomy. For each ROI, five DECT parameters were obtained and recorded: CT numbers (in HU) at low (80 kV) and high (140 kV) tube potentials, dual-energy index (DEI), electron density (Rho or $\rho_e$), and $Z_{eff}$. A random selection of 20 cases were independently measured by a musculoskeletal radiologist and remeasured by the first observer to assess inter- and intraobserver reliability.

### *Statistical analysis*

Data were analyzed using R (version 3.4.2; R Foundation for Statistical Computing, Vienna, Austria). Qualitative variables were reported as numbers (%), while quantitative variables as mean ± standard deviation (SD). Patient characteristics between CPPD and control groups were compared using Student t or Wilcoxon–Mann–Whitney tests and chi-squared or Fisher exact tests, where appropriate. Given repeated measurements on each subject, the different knee structures were compared using linear mixed models, considering patients as random effect and age as fixed effect when adjusting for confounders. Clinically relevant 2 × 2 comparisons (number and arrangement of pairs) were predefined, thereby limiting the number of tested null hypotheses. The model validation was assessed graphically using residuals (normality and homoscedasticity). When conditions were not satisfied even after log-transformation, permutation tests were implemented to estimate *p*-values with 20,000 permutations. *P*-values were corrected for each pairwise comparison at fixed DECT parameter using Holm's technique to avoid $\alpha$ risk inflation due to repeated comparisons between knee structures. Measurement reliability was assessed by computing intraclass correlation coefficients (ICC) with their 95% confidence intervals (95% CI), which were interpreted as follows: >0.8, very good; 0.61–0.8, good; 0.41–0.6, moderate; 0.21–0.4, fair; and ≤0.2, poor. Significance level was set at 5%.

## Results

### *Patient characteristics*

Patient characteristics overall as well as in CPPD patients and controls separately are detailed in Table I.

Both patient groups were comparable, except for age ($p = 0.007$) and radiographic chondrocalcinosis ($p < 0.0001$) (as well as history of acute CPP crystal arthritis and knee DECT chondrocalcinosis by study design). Overall, the 89 meniscal calcifications assessed in CPPD patients measured 0.20 ± 0.19 $cm^2$.

### *In-vivo DECT attenuation properties of meniscal calcifications in CPPD patients, and non-calcified menisci, subchondral and trabecular bone in CPPD patients and controls*

CT numbers at 80 and 140 kV, DEI, $\rho_e$, and $Z_{eff}$ of meniscal calcifications in CPPD patients, and non-calcified menisci, subchondral and trabecular bone in both CPPD patients and controls are reported in Table II.

**Table I**
Demographic and clinical characteristics of patients overall as well as in calcium pyrophosphate deposition (CPPD) patients and controls

| | Overall ($n = 40$) | CPPD patients ($n = 19$) | Controls ($n = 21$) | *P*-values |
|---|---|---|---|---|
| Gender (male/female) | 30/10 | 12/7 | 18/3 | 0.15* |
| Age (years) | 69 ± 13 | 75 ± 13 | 64 ± 11 | 0.007† |
| Body mass index (kg/m$^2$) | 28.5 ± 5.1 | 28.6 ± 5.5 | 28.3 ± 4.9 | 0.86‡ |
| Knee osteoarthritis | 20/40 (50%) | 11/19 (57.9%) | 9/21 (42.9%) | 0.53§ |
| Gout | 26/40 (65%) | 9/19 (47.4%) | 17/21 (81%) | 0.06§ |
| History of acute CPP crystal arthritis | 12/40 (30%) | 12/19 (63.2%) | 0/21 (0%) | N/A |
| Identification of CPP crystals in synovial fluid | 8/40 (20%) | 8/19 (42.1%) | 0/21 (0%) | N/A |
| Radiographic chondrocalcinosis (wrist and/or pelvis) | 16/34 (47.1%) | 14/16 (87.5%) | 2/18 (11.1%) | <0.0001* |

N/A = not applicable.
* Fisher exact test.
† Student *t*-test.
‡ Wilcoxon–Mann–Whitney test.
§ chi-squared test.

Values for all five DECT parameters were comparable between non-calcified menisci in CPPD patients ($n = 25$) and controls ($n = 126$) (all $p \geq 0.08$), as well as for subchondral (all $p \geq 0.20$) and trabecular bone (all $p \geq 0.32$) between CPPD patients ($n = 19$) and controls ($n = 21$).

*DECT can discriminate meniscal CPP deposits from non-calcified menisci and calcium HA in subchondral and trabecular bone*

The combined effects of volumetric mass density and $Z_{eff}$ on CT numbers at 80 and 140 kV, along with their discrimination potential, are illustrated in Fig. 1.

Meniscal calcifications were readily distinguished from non-calcified menisci in both CPPD patients (all $p < 0.0001$) and controls (all $p < 0.0001$) (Table II and Figs. 1 and 2). Meniscal CPP deposits were also easily differentiated from calcium HA in subchondral (all $p < 0.0001$) and trabecular bone ($p < 0.001$), except when using CT numbers at 80 kV separately ($p = 0.74$) (Fig. 2).

The same held true for both $Z_{eff}$ and $\rho_e$ in a subgroup analysis of CPPD patients with crystal-proven acute CPP crystal arthritis ($n = 8$) (all $p < 0.0001$).

*Measurement reliability*

Inter- and intraobserver reliability of $Z_{eff}$ measurements ranged between good and very good for all different knee structures (ICC = 0.76(0.62,0.85)-0.83(0.73,0.89) and 0.80(0.61,0.89)-0.91(0.85,0.94), respectively) and the delineation of meniscal calcification cross-sectional areas (ICC = 0.74(0.65,0.81) and 0.86(0.79,0.90), respectively).

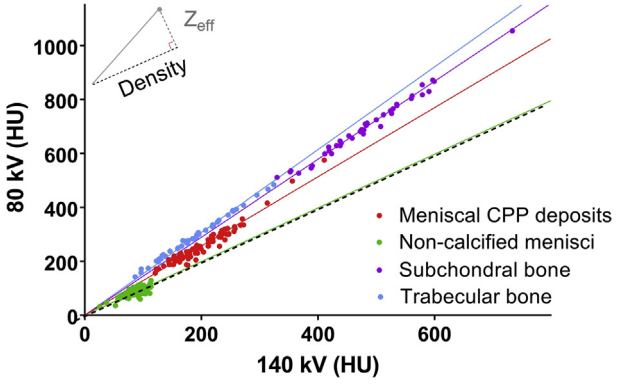


**Fig. 1.** Combined effects of volumetric mass density and effective atomic number ($Z_{eff}$) on CT numbers at 80 and 140 kV for meniscal calcifications in calcium pyrophosphate deposition (CPPD) patients, and non-calcified menisci, subchondral and trabecular bone in both CPPD patients and controls. The slope of each material is correlated with its $Z_{eff}$ and photoelectric effect; the steeper the slope, the higher the discrimination potential using dual-energy CT (DECT). HU = Hounsfield unit.

## Discussion

This initial clinical study shows that CPP crystal deposits exhibit specific DECT attenuation properties *in vivo* that enable to discriminate them from calcium HA in subchondral and trabecular bone, as well as non-calcified menisci, through their biochemical signatures. This may represent a pivotal step not only for the more widespread clinical use of DECT for diagnosing complex CPPD cases (e.g., improved detection in regions with normal plain radiographs and difficult synovial fluid aspiration, or in the spine), but also and more importantly for providing a better understanding and deeper insights into the pathogenic role that various calcium crystals (CPP vs basic calcium phosphates (BCP)) play within joints *in vivo*, particularly in OA[10].

Although DECT can differentiate intra-articular CPP deposits from calcium HA in bone, its sensitivity to detect small amounts of crystal aggregates *in vivo* remains to be investigated. Tanikawa *et al.* recently assessed the diagnostic performance of DECT, in comparison with conventional radiography, for detecting CPP crystal deposits in human knee menisci harvested at the time of total knee

**Table II**
*In-vivo* dual-energy computed tomography (DECT) attenuation properties of meniscal calcifications in CPPD patients, and non-calcified menisci, subchondral and trabecular bone in both CPPD patients and controls

| | *n* | CT numbers 80 kV (HU) | CT numbers 140 kV (HU) | Dual-energy index (DEI) | Electron density ($\rho_e$) | Effective Z number ($Z_{eff}$) |
|---|---|---|---|---|---|---|
| Meniscal calcifications in CPPD patients | 89 | 257 ± 64 | 201 ± 48 | 0.023 ± 0.007 | 140 ± 35 | 8.8 ± 0.3 |
| Non-calcified menisci in CPPD patients | 25 | 91 ± 19 | 88 ± 17 | 0.001 ± 0.005 | 76 ± 18 | 7.6 ± 0.2 |
| Non-calcified menisci in controls | 126 | 87 ± 13 | 88 ± 12 | 0.000 ± 0.004 | 79 ± 15 | 7.5 ± 0.2 |
| Subchondral bone | 40 | 701 ± 115 | 486 ± 83 | 0.067 ± 0.007 | 285 ± 60 | 10.8 ± 0.3 |
| Trabecular bone | 40 | 289 ± 84 | 187 ± 60 | 0.041 ± 0.008 | 91 ± 38 | 9.6 ± 0.4 |

*n* = number, HU = Hounsfield unit.

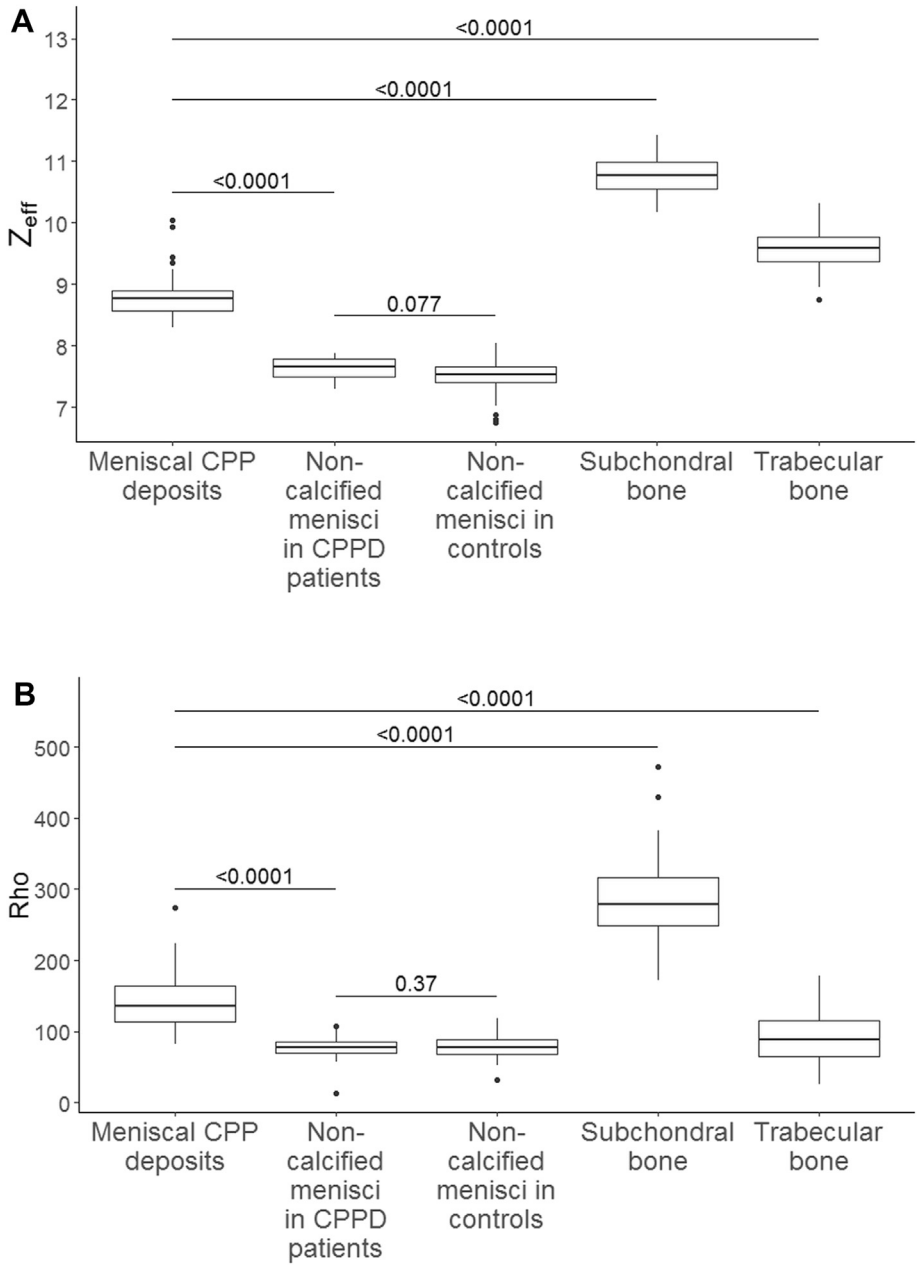


**Fig. 2.** Specific effects of effective Z number ($Z_{eff}$, A) and electron density (Rho or $\rho_e$, B) on material differentiation between meniscal calcifications in CPPD patients, and non-calcified menisci, subchondral and trabecular bone in both CPPD patients and controls. Relevant *p*-values are indicated above the corresponding box-and-whisker plots.

arthroplasty[14]. They found that DECT was more sensitive but less specific than plain radiographs (in our series, 2/15 (13.3%) available knee radiographs did not show chondrocalcinosis identified with DECT), and had an overall diagnostic accuracy in the same range as conventional CT[15]. This highlights the key fact that DECT is not primarily intended to enhance the detection of CPPD but rather to aid in characterizing calcium crystal aggregates, through intrinsic variations in $Z_{eff}$ and thus photoelectric effect (Fig. 1). Advances in detection of calcium and MSU crystal deposits are expected with the advent of multi-energy spectral photon-counting CT systems, which offer increased 3D spatial resolution (around 100 μm) with less partial volume effects, on top of operating at lower energy ranges (down to 15–20 keV, compared with 40 keV for DECT)[10,16,17].

The main advantage of DECT, as demonstrated here, lies in its ability to evaluate the biochemical signature of anatomical and pathological structures in the human body. In particular, DECT attenuation properties of meniscal CPP deposits were statistically significantly different from those of calcium HA in subchondral and trabecular bone, the latter sharing as expected very similar $Z_{eff}$ and photoelectric effect (reflected by their slopes in Fig. 1) while exhibiting different densities (reflected by their distances from the origin). Conversely, meniscal CPP and calcium HA in trabecular bone shared similar densities but were readily distinguished owing to different $Z_{eff}$ and photoelectric effect, as shown by the clear separation of the corresponding point clouds in Fig. 1.

The ability of DECT to characterize the various types of calcium-containing crystals within and around joints would be a step forward in clarifying the role of comorbid calcium crystal deposition in OA[2]. Using conventional CT, there is still conflicting evidence regarding the correlation between knee chondrocalcinosis and OA,

although intra-articular calcification was reported to be universal while predominating in meniscal fibrocartilage[15,18]. Furthermore, in an ex-vivo study of human knee OA articular cartilage with Fourier-transform infrared spectroscopy and scanning electron microscopy, Nguyen *et al.* demonstrated that calcium-containing crystals were always present in OA cartilage[19]. Calcifications comprised BCP crystals at all times, which coexisted with CPP crystals in approximately 40% of cases. Utilizing the potential of DECT to non-invasively discriminate CPP from BCP crystal deposits *in vivo* would be a major advance in this field of research and could enable the development of targeted therapies that are currently lacking[1,4].

We acknowledge the following study limitations. First, and most importantly, not all CPPD patients had microscopic confirmation of CPP crystals in synovial fluid aspirates; yet this reference standard is notoriously not perfect[20] and a subgroup analysis with only crystal-proven cases reached the same conclusions. Previous cadaveric studies confirmed using Fourier-transform infrared spectroscopy that calcium deposits in knees with chondrocalcinosis were predominantly made of CPP crystals[21]. It is however likely that meniscal calcifications in CPPD patients also contain a certain amount of calcium HA, even though maybe not high enough to result in statistically significant differences in density and/or $Z_{eff}$[19]. Without direct examination of the menisci for calcium crystal deposits, we were thus unable to assess the extent and impact of crystal deposition heterogeneity. Further studies will have to address this important limitation using an accurate reference standard and/or calibrated DECT crystal samples. Second, the sample size of this initial clinical experience was too small to determine whether non-calcified menisci of CPPD patients at imaging had a different DECT biochemical signature than those of control patients. Third, a substantial number of CPPD patients and controls had coexisting gout. However, MSU exhibits no photoelectric effect and thus shares DECT attenuation properties very similar to non-calcified menisci. Fourth, the spatial resolution of DECT was relatively limited compared to the small size of meniscal calcifications. However, we took special care to avoid partial volume effects, and found good to very good measurement reliability. Furthermore, there was a weak-very weak association between the size of the measured meniscal calcifications and DECT parameters, in particular $Z_{eff}$ and $\rho_e$ (Spearman's correlation coefficient = 0.39(0.21,0.56) and 0.13(-0.09,0.34); data not shown). Finally, although our results are derived from basic DECT parameters (DEI, $\rho_e$, and $Z_{eff}$), we were unable to test their application using a proprietary material decomposition image reconstruction algorithm, such as those currently available for gout. These findings should now be incorporated into such post-processing tools to enable rapid semi-automated use and analysis of DECT scans in clinical practice, with non-invasive quantification and color-coded mapping of intra- and juxta-articular calcium crystal deposits.

In conclusion, this proof-of-concept study shows that DECT has the potential to discriminate meniscal CPP deposits from calcium HA in subchondral and trabecular bone *in vivo*, paving the way for the non-invasive biochemical signature assessment of intra- and juxta-articular calcium crystal deposits.

## Author contributions

Tristan Pascart – study conception and design, data acquisition, analysis and interpretation, manuscript drafting, revision and final approval.

Laurène Norberciak – data analysis and interpretation, manuscript revision and final approval.

Julie Legrand – data analysis, manuscript revision and final approval.

Fabio Becce – study conception and design, data interpretation, manuscript drafting, revision and final approval.

Jean-François Budzik – study conception and design, data acquisition and interpretation, manuscript revision and final approval.

## Competing interest statement

None of the authors has any conflict of interest to disclose regarding this study.

## Source of funding

None.

## Supplementary data

Supplementary data to this article can be found online at https://doi.org/10.1016/j.joca.2019.05.007.

## References

1. McCarthy GM, Dunne A. Calcium crystal deposition diseases - beyond gout. Nat Rev Rheumatol 2018;14:592–602.
2. Nalbant S, Martinez JA, Kitumnuaypong T, Clayburne G, Sieck M, Schumacher Jr HR. Synovial fluid features and their relations to osteoarthritis severity: new findings from sequential studies. Osteoarthritis Cartilage 2003;11:50–4.
3. Zhang W, Doherty M, Bardin T, Barskova V, Guerne PA, Jansen TL, *et al.* European League against Rheumatism recommendations for calcium pyrophosphate deposition. Part I: terminology and diagnosis. Ann Rheum Dis 2011;70:563–70.
4. Abhishek A, Neogi T, Choi H, Doherty M, Rosenthal AK, Terkeltaub R. Unmet needs and the path forward in joint disease associated with calcium pyrophosphate crystal deposition. Arthritis Rheum 2018;70:1182–91.
5. Freire V, Moser TP, Lepage-Saucier M. Radiological identification and analysis of soft tissue musculoskeletal calcifications. Insights Imaging 2018;9(4).
6. Banks KP, Bui-Mansfield LT, Chew FS, Collinson F. A compartmental approach to the radiographic evaluation of soft-tissue calcifications. Semin Roentgenol 2005;40:391–407.
7. Omoumi P, Becce F, Racine D, Ott JG, Andreisek G, Verdun FR. Dual-energy CT: basic principles, technical approaches, and applications in musculoskeletal imaging (Part 1). Semin Musculoskel Radiol 2015;19:431–7.
8. Choi HK, Al-Arfaj AM, Eftekhari A, Munk PL, Shojania K, Reid G, *et al.* Dual energy computed tomography in tophaceous gout. Ann Rheum Dis 2009;68:1609–12.
9. Araujo EG, Bayat S, Petsch C, Englbrecht M, Faustini F, Kleyer A, *et al.* Tophus resolution with pegloticase: a prospective dual-energy CT study. RMD Open 2015;1, e000075.
10. Becce F. Diagnosis of calcium pyrophosphate deposition by imaging - current state and challenges remaining. Osteoarthritis Cartilage 2019;27:545–6.
11. Neogi T, Jansen TL, Dalbeth N, Fransen J, Schumacher HR, Berendsen D, *et al.* 2015 gout classification criteria: an American college of rheumatology/european league against rheumatism collaborative initiative. Arthritis Rheumatol 2015;67:2557–68.
12. Pascart T, Grandjean A, Norberciak L, Ducoulombier V, Motte M, Luraschi H, *et al.* Ultrasonography and dual-energy computed tomography provide different quantification of urate burden in gout: results from a cross-sectional study. Arthritis Res Ther 2017;19:171.
13. Almeida IP, Schyns LE, Ollers MC, van Elmpt W, Parodi K, Landry G, *et al.* Dual-energy CT quantitative imaging: a

comparison study between twin-beam and dual-source CT scanners. Med Phys 2017;44:171–9.
14. Tanikawa H, Ogawa R, Okuma K, Harato K, Niki Y, Kobayashi S, *et al*. Detection of calcium pyrophosphate dihydrate crystals in knee meniscus by dual-energy computed tomography. J Orthop Surg Res 2018;13:73.
15. Misra D, Guermazi A, Sieren JP, Lynch J, Torner J, Neogi T, *et al*. CT imaging for evaluation of calcium crystal deposition in the knee: initial experience from the Multicenter Osteoarthritis (MOST) study. Osteoarthritis Cartilage 2015;23:244–8.
16. Stamp LK, Anderson NG, Becce F, Rajeswari M, Polson M, Guyen O, *et al*. Clinical utility of multi-energy spectral photon-counting CT in crystal arthritis. Arthritis Rheum 2019;71, https://doi.org/10.1002/art.40848.
17. Kirkbride TE, Raja AY, Muller K, Bateman CJ, Becce F, Anderson NG. Discrimination between calcium hydroxyapatite and calcium oxalate using multienergy spectral photon-counting CT. AJR Am J Roentgenol 2017;209:1088–92.
18. Touraine S, Ea HK, Bousson V, Cohen-Solal M, Laouisset L, Chappard C, *et al*. Chondrocalcinosis of femoro-tibial and proximal tibio-fibular joints in cadaveric specimens: a high-resolution CT imaging study of the calcification distribution. PLoS One 2013;8, e54955.
19. Nguyen C, Bazin D, Daudon M, Chatron-Colliet A, Hannouche D, Bianchi A, *et al*. Revisiting spatial distribution and biochemical composition of calcium-containing crystals in human osteoarthritic articular cartilage. Arthritis Res Ther 2013;15:R103.
20. Berendsen D, Neogi T, Taylor WJ, Dalbeth N, Jansen TL. Crystal identification of synovial fluid aspiration by polarized light microscopy. An online test suggesting that our traditional rheumatologic competence needs renewed attention and training. Clin Rheumatol 2017;36:641–7.
21. Ryu K, Iriuchishima T, Oshida M, Kato Y, Saito A, Imada M, *et al*. The prevalence of and factors related to calcium pyrophosphate dihydrate crystal deposition in the knee joint. Osteoarthritis Cartilage 2014;22:975–9.